

Enhancement of dynamic wireless power transfer system by model predictive control

Ali Alkadir¹ | Seyed Ehsan Abdollahi¹  | Seyed Reza Abdollahi² | Patrick Wheeler³

¹ Electrical and Computer Engineering, Babol Noshirvani University of Technology, Shariati Av, Babol, Iran

² Electrical and Computer Engineering, University of Science and Technology of Mazandaran, University Blv, Behshahr, Iran

³ Electrical and Electronic Engineering, University of Nottingham, Nottingham, UK

Correspondence

Seyed Ehsan Abdollahi, Electrical and Computer Engineering, Babol Noshirvani University of Technology, Shariati Av, Babol, Iran.
Email: e.abdollahi@nit.ac.ir

Abstract

Wireless power transfer (WPT) system based on a dynamic wireless charging (DWC) scheme, eliminates waiting time for charging electric vehicles (EVs), increases the range of motion, reduces the size of Li-ion battery, and automates the charging process. In the DWC method, an EV frequently passes the charger transmitter pads at maximum speed to charge the onboard battery. The charger must have a quick and smooth transient response that employs the proper charging strategy for the battery. Here, a model predictive controller (MPC) is proposed to deploy a suitable DWC based on constant current/voltage (CC/CV) charging protocol. The designed MPC functionality is demonstrated by simulation and experimental results for both CC/CV strategies while battery state of charge (SOC) is estimated by a simple and stable technique in the primary side. The applied CC/CV MPC scheme performs properly in all conditions with a fast critically damped start-up, which makes it a potential choice to charge EV in dynamic and static modes. The simulation results of the proposed controller are verified by implementing a 90 W WPT testbed at 85.5 kHz switching frequency and 100 mm coils' air gap.

1 | INTRODUCTION

The WPT has drawn much attention in recent years due to its convenience, safe and fully automatic access to electrical power [1]. The WPT technology is used in many applications such as medical implants [2, 3], consumer electronics [4, 5] and robotics [6, 7]. Because of the abovementioned advantages, WPT is a good choice to replace the plug-in EV charger in static wireless charging (SWC) [8, 9]. As shown in Figure 1a, the dynamic wireless charging (DWC) for EV is a promising solution to extend driving range, decreases the battery size and eliminates the waiting time for charging [1].

Due to the superior energy density of Li-ion batteries, they are widely used as EV energy storage systems. Since, they are very sensitive to overvoltage [10], the WPT system controller in both CC/CV charging modes should regulate current/voltage smoothly and especially at start-up.

According to Figure 1b, at the beginning of the CC/CV charging process, the battery is charged with CC mode. Nominal current is applied to the battery continuously ($I_o = I_{ref}$) until the output voltage reaches the nominal voltage of the battery

($V_o = V_{ref}$). Then, to avoid increasing the output voltage (V_o) over the reference voltage (V_{ref}), the charging process changes from CC to CV mode. In this mode, V_o remains equal to V_{ref} , and when the charging process is completed ($I_o < 0.1 I_{ref}$), the system turns off. During the charging, the SOC of the battery increases and can be modelled as an equivalent load resistance (R_o , as shown with purple line in Figure 1b) [11–13]. In [14, 15], hybrid topologies in the primary and secondary sides are implemented to achieve CC/CV modes without requiring feedback control. These methods need additional inductors, capacitors, switches, and controller which increase the complexity, cost, and uncertainty of the system.

A WPT system has a high-frequency inverter, loosely-coupled transformer, high-order resonance tank, and other non-linear elements. In [11, 16, 17] a conventional proportional-integral (PI) controller was proposed to achieve CC/CV charging scheme and improve dynamic performance of WPT system respectively. But according to the inherent characteristics of the PI controller (linearity and simple mathematical model), its dynamic performance is limited. In [18], they worked on improving the dynamic performance of maximum energy

This is an open access article under the terms of the [Creative Commons Attribution](https://creativecommons.org/licenses/by/4.0/) License, which permits use, distribution and reproduction in any medium, provided the original work is properly cited.

© 2021 The Authors. *IET Power Electronics* published by John Wiley & Sons Ltd on behalf of The Institution of Engineering and Technology

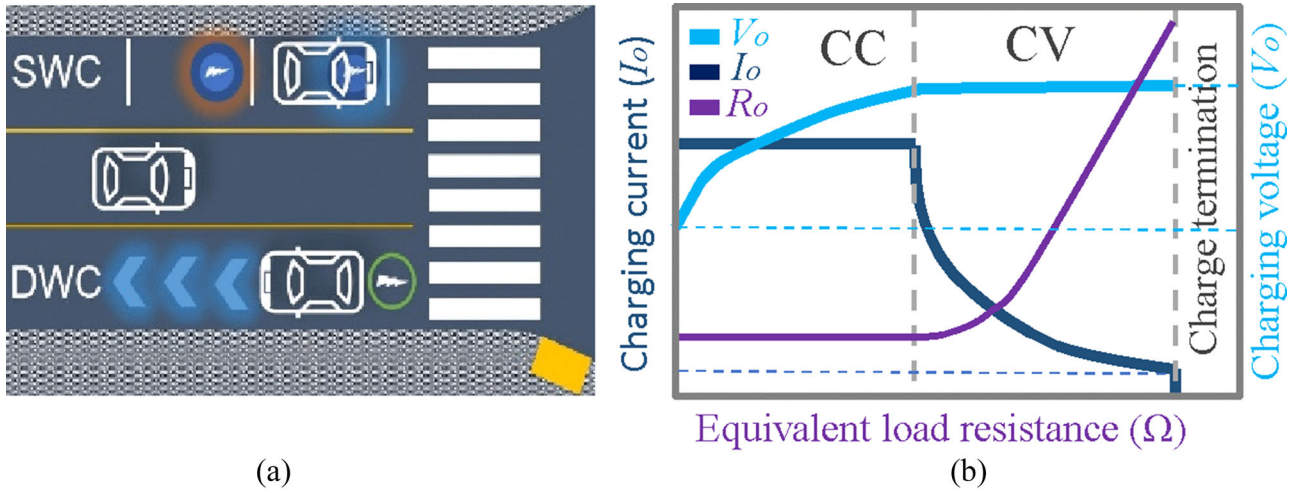


FIGURE 1 (a) Dynamic and static EV wireless charging and (b) CC/CV charging protocol of a Li-ion battery

efficiency tracking by using a sliding mode controller in the secondary side. The system required two controllers (in primary and secondary side) as well as a secondary boost converter, which increases the complexity and cost of the system. In [19], based on impedance matching a mutual inductance estimation strategy is used for DWC system to obtain maximum efficiency while regulating the output voltage of the WPT system. The impedance matching method requires bulky inductors or capacitors which increases control complexity and size of the WPT system [20]. In [21, 22], controllers based on one cycle-PD and switching control strategy are proposed to improve the transient response. High complexity of the WPT system makes it difficult to effectively implement the proposed control strategy. In [23], a deep learning controller is used to improve the transient response of the WPT system. A sliding mode controller is used to estimate system dynamics, two deep neural networks to eliminate the sliding mode controller estimation error and a feed-back controller to stabilize voltage response of the DC-DC converter. As a result, the controller is complex (and hard to design). Furthermore, [23] not only it lacks the output current regulation which is very important for the Li-ion battery but also it requires an additional DC-DC converter to implement the controller. In this paper, a model predictive controller (MPC) is proposed to improve system transient response. This controller is a simple and powerful controller based on the optimal control scheme with fast, and accurate dynamic response [24]. In addition, it is proper for a nonlinear system that does not need to tune the gain of the controller which is essential in system with PI controllers. In [21], MPC is employed to ensure the reliable operation of the WPT system in case of a quick change in coupling coefficient. In [25–27], MPC is used to improve the performance of a bidirectional WPT system for maximum efficiency tracking and power flow process.

The main contribution of this paper is to deploy a primary-side MPC for the WPT system to execute CC/CV protocol with a fast and smooth dynamic transient response. Based on the proposed estimation technique of the SOC of the

Li-ion battery, there is no need to a communication link to feedback state of the secondary side to the primary side. Because of the fast and smooth start-up transient response of the proposed controller; it is suitable for dynamic and static wireless charging. Smooth transient avoids damage to the Li-ion battery and fast turn on/off system makes the system suitable for high-speed mobility of the EVs over charging pads. The H-bridge inverter through phase-shift modulation (PSM) technique with a constant switching frequency regulates the output voltage/current. Simulation and experimental results validate the smooth, quick transient, and accurate steady-state response of the proposed controller. Due to the simplicity and applicability, the series-series (SS) resonant tank is used in this work. The rest of this paper is organized as follows: In section 2 the WPT structure and fundamental theoretical analysis of the WPT system are presented. Section 3 presents the proposed load estimation technique and the primary-side MPC scheme analysis and related simulations are discussed in Sections 4 and 5, respectively. Finally, Section 6 validates the proposed MPC technique with experimental results.

2 | SYSTEM CONFIGURATION

2.1 | System structure

WPT system has two electrical isolated sides: transmitter or grid side and receiver or EV side that are shown in Figure 2. The MPC is deployed in the primary side to achieve CC/CV protocol. The H-bridge inverter regulates the value of input voltage to the resonant tank through the phase shift technique. The source DC voltage is converted to high-frequency AC and applied to the primary series resonant tank as a transmitter. Then, it is transferred via magnetic coupling to the secondary series resonant tank as a receiver and after rectification, charges the Li-ion battery. Due to weak coupling between the transmitter and the receiver coils ($L1, L2$) reactive power is high,

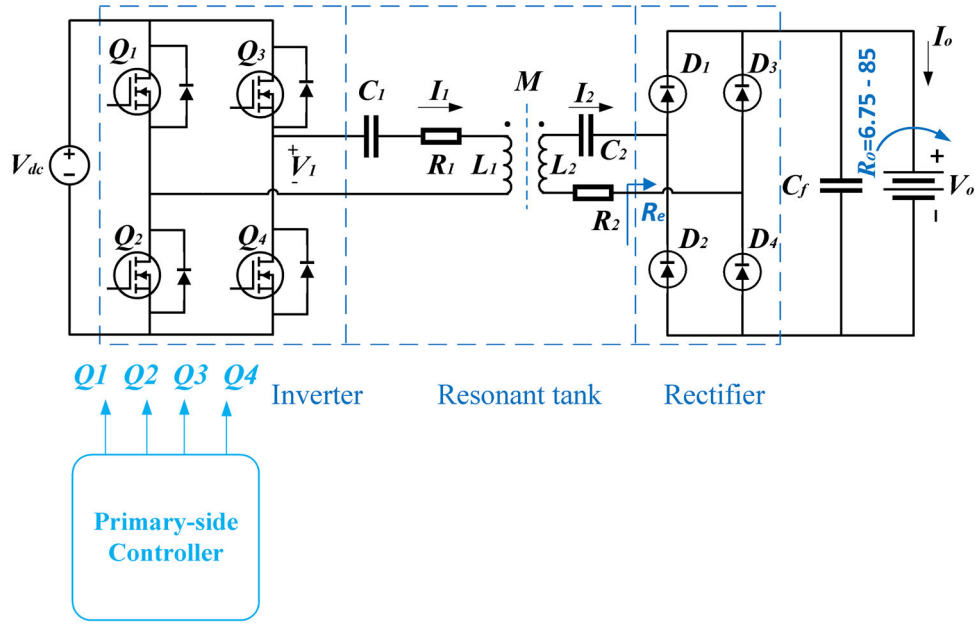


FIGURE 2 Structure of a WPT system

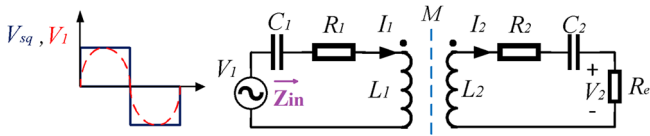


FIGURE 3 FHA approximation of the WPT circuit

therefore compensation capacitors (C_1 , C_2) are necessary to reduce the reactive power of the circuit. As a result, component VA rating is reduced and efficiency of the system is increased [28]. On the secondary side, a full-bridge rectifier and a capacitive filter are used to rectify and reduce the switching ripple of the charging current or voltage [29].

2.2 | Full-bridge inverter model

The square wave voltage is applied to the H-bridge inverter and the resonant tank includes multiple frequency components. For simplicity in the circuit analysis, an acceptable approximation is made to consider the first-order harmonic and ignore the other higher-order harmonics.

The name of this method is the first harmonic approximation (FHA), which produces a suitable design as long as the WPT converter operates at or close to the resonant frequency. The simplified circuit of Figure 2 based on FHA is shown in Figure 3.

where V_{sq} is the output inverter voltage and V_1 is FHA estimation of V_{sq} . The R_1 , R_2 , I_1 , I_2 , are primary and secondary winding resistances and tank currents, respectively. M , V_2 and R_e are the mutual inductance, the secondary side AC voltage, and the equivalent load resistance at the input of the rectifier,

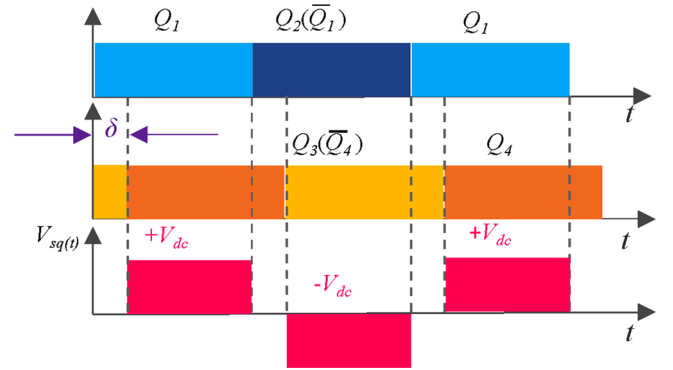


FIGURE 4 The output voltage of the H-bridge inverter (pink) and MOSFET gate signals of the H-bridge (blue, orange)

respectively. The RMS value of V_1 is:

$$V_{1,rms} = \frac{2\sqrt{2}}{\pi} V_{dc} \cos\left(\frac{\delta}{2}\right) \quad (1)$$

where δ is the phase shift angle between the switching pulse of each leg of the H-bridge inverter (Figure 4). Any changes in the δ , leads to a change in the duty cycle of the inverter voltage. It causes the output voltage/ current to be adjusted. The δ is changed from 0 to π radian, which is equivalent to change of the duty cycle from 50 to 0%.

2.3 | Output rectifier model

Because in WPT application, battery charging operation is slow and applied voltage and current are dc, the Li-ion battery can

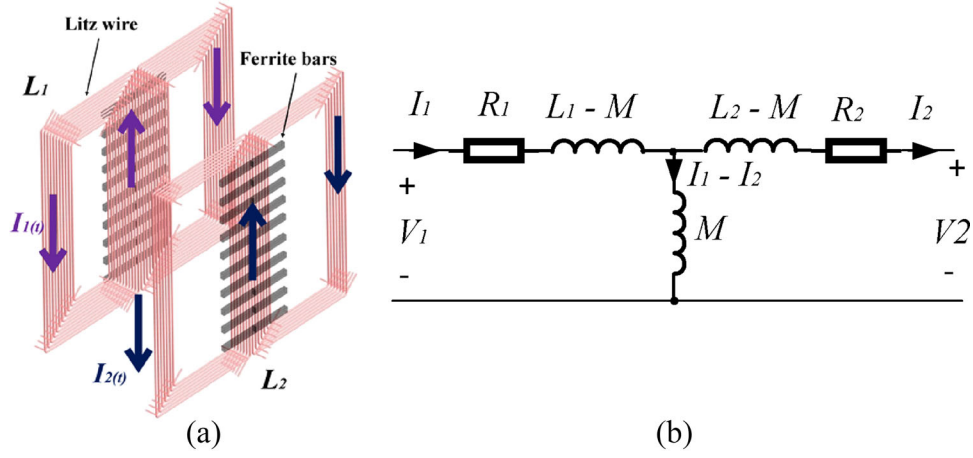


FIGURE 5 Power pads (a) structure of DD type pads (b) electrical T-model of the DD pads

be modelled as a variable resistor R_o [11, 12]. The equivalent resistance and RMS voltage/current of the input rectifier view are R_e , $V_{2,rms}$ and $I_{2,rms}$, respectively.

$$R_e = \frac{8}{\pi^2} R_o \quad (2)$$

$$V_{2,rms} = \frac{2\sqrt{2}}{\pi} V_o \quad (3)$$

$$I_{2,rms} = \frac{\pi}{2\sqrt{2}} I_o \quad (4)$$

2.4 | Magnetic coupler model

Generally, in high power WPT applications like EV charging, the loosely coupled transformer consists of ferrite cores and litz copper coils (Figure 5a). The T-model of loosely-coupled transformer is presented in Figure 5b. The magnetic losses and nonlinearities of the core are ignored and just resistive losses of the primary and secondary coils are considered in the model. The above-mentioned assumptions are acceptable in the inductive WPT system [30, 31].

The mutual inductance that is defined by coupling factor (k) and self-inductances is expressed as:

$$M = k\sqrt{L_1 L_2} \quad (5)$$

The mutual inductance depends on the shape and the material of the WPT system's transmitter and receiver pads, and alignment between them. Figure 6 shows finite element method (FEM) simulation of the mutual inductance (M) of the DD power pads under X and Y -axes misalignment. According to the figure, it can be concluded that the DD structure is more robust to displacement along the Y -axis direction, so the EV must move along the Y -axis direction [32].

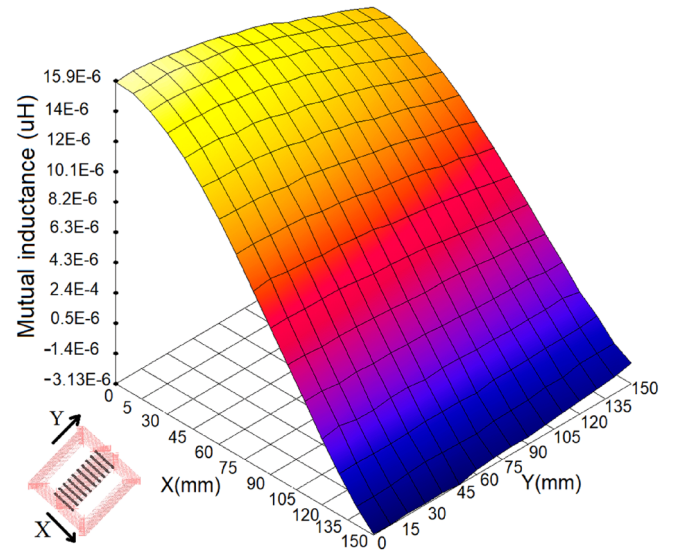


FIGURE 6 Mutual inductance of DD pads under misalignment along x and y -axes

2.5 | Resonant tank model

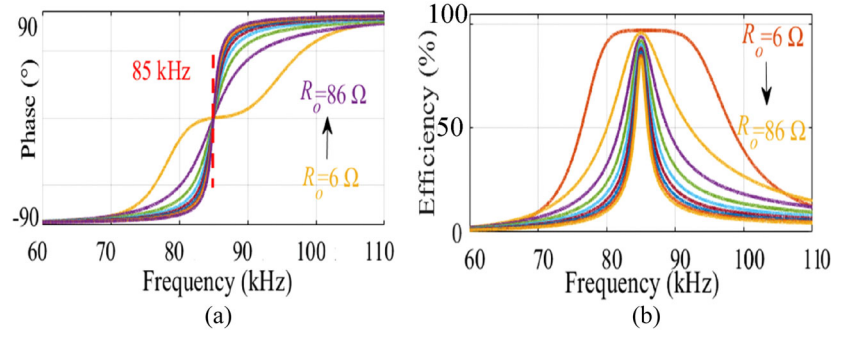
By applying the Kirchhoff voltage law (KVL) in Figure 3 the relationship between input voltage/current and output voltage/current is given by:

$$\begin{bmatrix} \vec{V}_1 \\ 0 \end{bmatrix} = \begin{bmatrix} Z_1 & Z_{12} \\ Z_{12} & Z_2 \end{bmatrix} \begin{bmatrix} \vec{I}_1 \\ \vec{I}_2 \end{bmatrix} \quad (6)$$

where primary, secondary, and mutual impedance are given by:

$$\begin{cases} Z_1 = R_1 + j\omega L_1 + \frac{1}{j\omega C_1}, & Z_{12} = -j\omega M \\ Z_2 = R_2 + j\omega L_2 + \frac{1}{j\omega C_2} + R_e \end{cases} \quad (7)$$

FIGURE 7 The frequency response under all range of load (6–86 Ω) (a) phase of Z_{in} (b) efficiency



where $\omega = 1/\sqrt{L_1 C_1} = 1/\sqrt{L_2 C_2}$ is the switching angular frequency of the inverter. The primary and secondary side ac currents can be calculated as:

$$\vec{I}_1 = \frac{Z_2}{Z_1 Z_2 - Z_{12}^2} \vec{V}_1 \quad (8)$$

$$\vec{I}_2 = \frac{Z_{12}}{Z_{12}^2 - Z_1 Z_2} \vec{V}_1 \quad (9)$$

From Equation (9), the magnitude of I_2 can be changed by changing the voltage V_1 . According to Equation (1), the amplitude of the voltage V_1 can be modified by changing the value of the δ . This changes the output current I_o according to Equations (4) and (9). The output voltage V_o can be adjusted where, $V_o = R_o I_o$. The R_o has a variable value which is related to the SOC of the battery and it needs to be estimated.

2.6 | Characteristics of SS resonant tank

It can be seen in Figure 7a as the R_o changes from 6 to 86 Ω , at resonance frequency, the system phase angle for all the loads remains zero. Figure 7b shows the efficiency under load and frequency variations. For all the loads, the highest system efficiency occurs at the resonance frequency. When the resistance R_o grows the phase angle of the impedance rises and power factor decreases, so it can be concluded that at light loads, the efficiency decreases.

The V_2 to V_1 and the I_2 to V_1 gains relationships are given by Equations (10) and (11):

$$Gain = \left| \frac{V_2}{V_1} \right| = \left| \frac{j\omega M R_e}{\omega^2 M^2 - \left(\omega L_2 - \frac{1}{\omega C_2}\right) \left(\omega L_1 - \frac{1}{\omega C_1}\right) + jR_e \left(\omega L_1 - \frac{1}{\omega C_1}\right)} \right| \quad (10)$$

$$Gain = \left| \frac{I_2}{V_1} \right| = \left| \frac{j\omega M}{\omega^2 M^2 - \left(\omega L_2 - \frac{1}{\omega C_2}\right) \left(\omega L_1 - \frac{1}{\omega C_1}\right) + jR_e \left(\omega L_1 - \frac{1}{\omega C_1}\right)} \right| \quad (11)$$

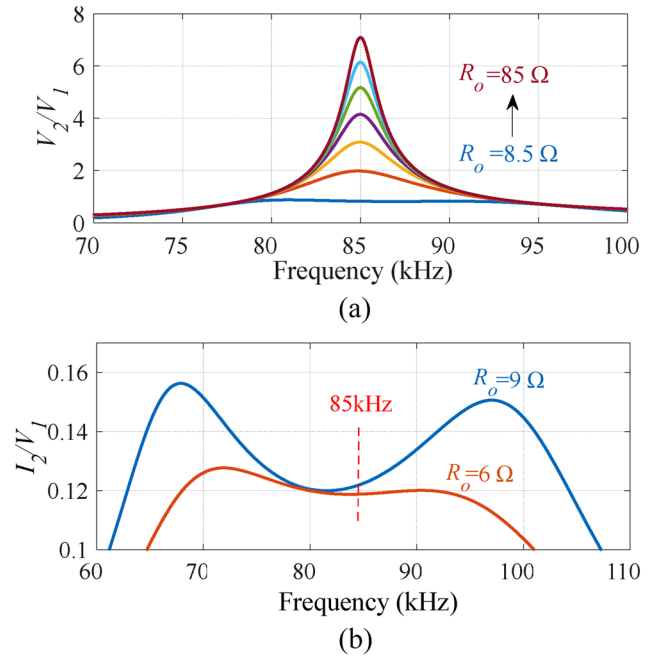


FIGURE 8 The frequency response of the system gain (a) output voltage gain (b) output current gain

As shown in Figure 8a,b, when the load resistance increases, the V_2/V_1 and I_2/V_1 gains of the circuit increase. So, the value of V_1 must be adjusted to keep the V_o and I_o at a desired value.

3 | LOAD ESTIMATION AND OUTPUT VOLTAGE/ CURRENT CALCULATION

In order to estimate the SOC of the Li-ion battery, the V_o and I_o need to be adjusted and the system turns on/off. A communication link is required to transfer load data to the primary side. The communication link increases the uncertainty, complexity and price of the system. Therefore, in this paper, with the aim of removing the communication link, the SOC of the battery is estimated based on the equivalent load resistance.

3.1 | Load estimation

According to the equivalent circuit of the WPT system in Figure 3, the input impedance at the source input and input active power P_1 are given by:

$$Z_{in} = R_1 + j\omega L_1 - j\frac{1}{\omega C_1} + \frac{\omega^2 M^2}{R_e + R_2 + j\omega L_2 - j\frac{1}{\omega C_2}}$$

$$\times \left[R_1 + \frac{\omega^2 M^2 (R_e + R_2)}{(R_e + R_2)^2 + \left(\omega L_2 - \frac{1}{\omega C_2}\right)^2} \right]$$

$$+ j \left[\omega L_1 - \frac{1}{\omega C_1} - \frac{\omega^2 M^2 \left(\omega L_2 - \frac{1}{\omega C_2}\right)}{(R_e + R_2)^2 + \left(\omega L_2 - \frac{1}{\omega C_2}\right)^2} \right]. \quad (12)$$

$$P_1 = I_{1,rms}^2 \operatorname{Re}(Z_{in})$$

$$= I_{1,rms}^2 \left[R_1 + \frac{\omega^2 M^2 (R_e + R_2)}{(R_e + R_2)^2 + \left(\omega L_2 - \frac{1}{\omega C_2}\right)^2} \right]. \quad (13)$$

The operating frequency is assumed to be equal to the resonance frequency (while at resonant frequency the Z_{in} is pure resistive). By Equation (13) and measured $I_{1,rms}$ the estimation of the load resistor R_o can be given by:

$$R_o = \frac{\pi^2}{8} \left[\frac{\omega^2 M^2 I_{1,rms}^2}{P_1 - R_1 I_{1,rms}^2} - R_2 \right]. \quad (14)$$

Figure 9 shows the set and estimated equivalent load resistance value. The R_o estimation shows good tracking with a maximum of 2.5% error.

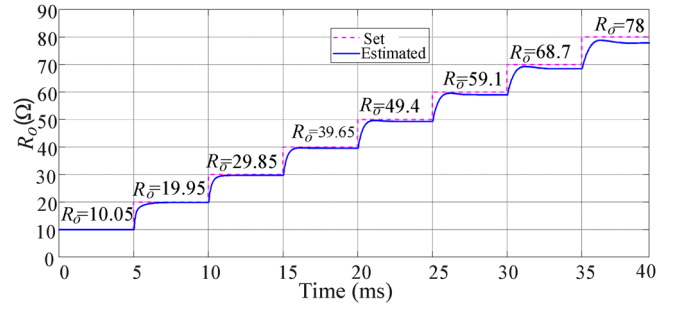


FIGURE 9 Simulation of the set (purple) and estimation (blue) equivalent load resistance

TABLE 1 Parameters of the WPT system

V_{dc}, V_o (CV)	36, 25.8 V	R_1, R_2	0.15, 0.1 Ω
I_{dc}, I_o (CC)	4, 3 A	C_1, C_2	33.55, 68.5 nF
R_o	6.75-8.5 (CC mode) 8.5-85 (CV mode)	L_1, L_2	104.5, 51.2 μH

3.2 | Output voltage and current calculation

In this section, the V_o and I_o are calculated. From Equations (1), (8) and assuming the operating frequency is equal to the resonant frequency the calculated $I_{1,rms}$ is given by:

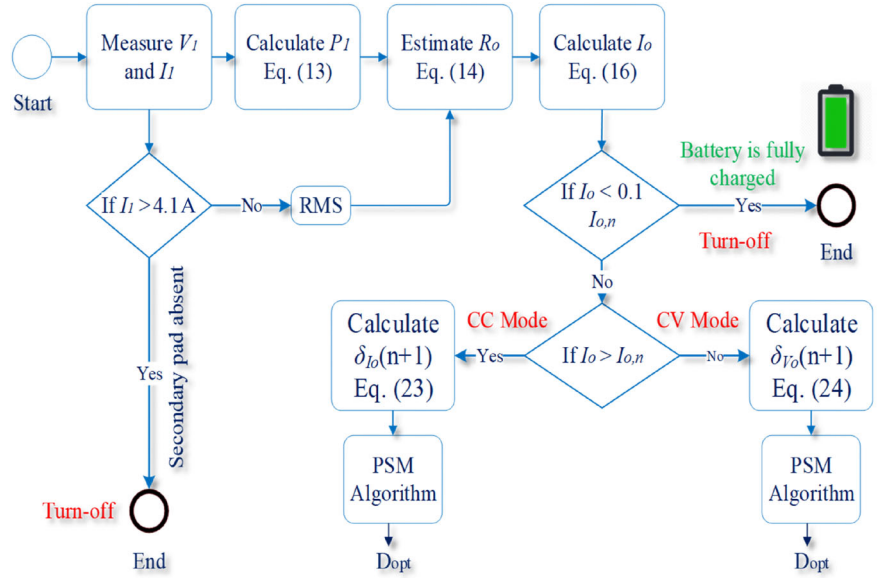
$$I_{1,rms} = \frac{2\sqrt{2}V_{dc} \cos\left(\frac{\delta}{2}\right)}{\pi \left(R_1 + \frac{\omega^2 M^2}{R_2 + R_e} \right)}. \quad (15)$$

The Equation (15) shows the relationship between R_o , δ and $I_{1,rms}$. According to Equation (15), by changing the value of δ , the duty cycle of V_1 changes, so $I_{1,rms}$ can be controlled by setting the δ . Furthermore, when the receiver power pad passes over the transmitter power pad, the mutual inductance decreases rapidly, as shown in Figure 6. Also from Equation (15) the primary side current increases more than nominal value and maybe damages the WPT system. Therefore, the system needs a current protection mechanism. By combining Equations (1), (4), (9) and (15), the I_o and the V_o can be calculated by:

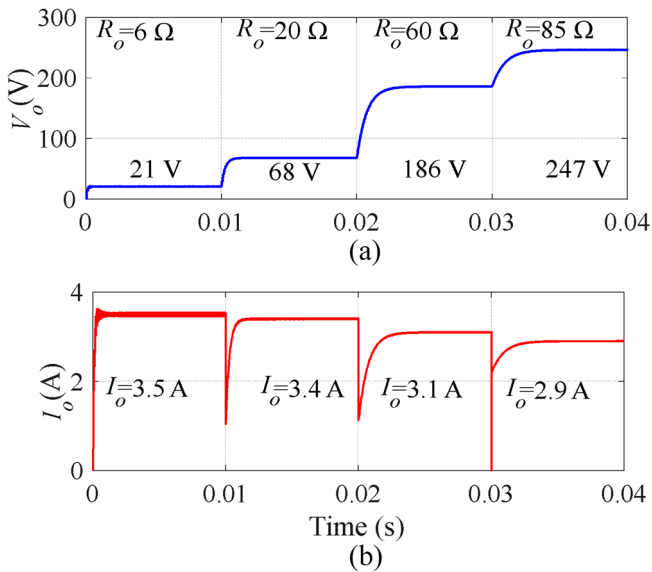
$$I_o = \frac{2\sqrt{2}I_{1,rms}\omega M}{\pi \sqrt{\left(\frac{\omega^2 L_2 C_2 - 1}{\omega C_2}\right)^2 + (R_2 + R_e)^2}}. \quad (16)$$

$$V_o = \frac{2\sqrt{2}R_o I_{1,rms}\omega M}{\pi \sqrt{\left(\frac{\omega^2 L_2 C_2 - 1}{\omega C_2}\right)^2 + (R_2 + R_e)^2}}. \quad (17)$$

According to Equations (16) and (17), the V_o and I_o are related to the primary side current and the value of the load.

FIGURE 10 Proposed algorithm to implement CC/CV method

TABLE 2 start-up transient responses of the PI and MPC (proposed)

Controller	CC Mode				CV Mode							
	$R_o = 7 \Omega$		$R_o = 8.4 \Omega$		$R_o = 8.6 \Omega$		$R_o = 40 \Omega$		$R_o = 60 \Omega$		$R_o = 85 \Omega$	
	Settling time	Over-shoot	Settling time	Over-shoot	Settling time	Over-shoot	Settling time	Over-shoot	Settling time	Over-shoot	Settling time	Over-shoot
PI	6 ms	0	10 ms	0%	12 ms	0%	18.2 ms	5.4 %	2.7 ms	15.5 %	2.7 ms	24 %
MPC (Proposed)	0.87 ms	0	1.45 ms	0%	1.7 ms	0%	1.2 ms	0 %	1.03 ms	0%	0.95 ms	2.3%


FIGURE 11 Open-loop simulation. (a) output voltage (b) output current

Therefore, the I_o and the V_o can be adjusted by controlling the input current $I_{1,rms}$ while $I_{1,rms}$ is controlled based on Equation (15) by adjusting the phase shift angle δ .

4 | PROPOSED PRIMARY-SIDE MPC SCHEME

4.1 | Primary-side MPC scheme

In this paper, MPC has been used with the aim of having fast and smooth start-up and mitigating the dynamic problem during load and mutual inductance changes in the WPT system with SS tank. The MPC scheme based on the system mathematical model, chooses an optimal response from the existing responses and applies it to set up the WPT system. The MPC is a simple, multi-objective and powerful method, which is based on the optimal control rules with a very fast and accurate response [33]. The MPC scheme can be formulated as:

$$J(N_1, N_p, N_c) = \sum_{k=N_1}^{N_p} \lambda(k) [y(n+k) - w(n+k)]^2 + \sum_{k=1}^{N_c} \alpha(k) [\Delta u(n+k)]^2. \quad (18)$$

where N_1 , N_p , N_c , $y(n)$, $w(n)$, Δu , $\lambda(k)$, $\alpha(k)$ are model delayed, prediction horizon, control horizon, model output, reference,

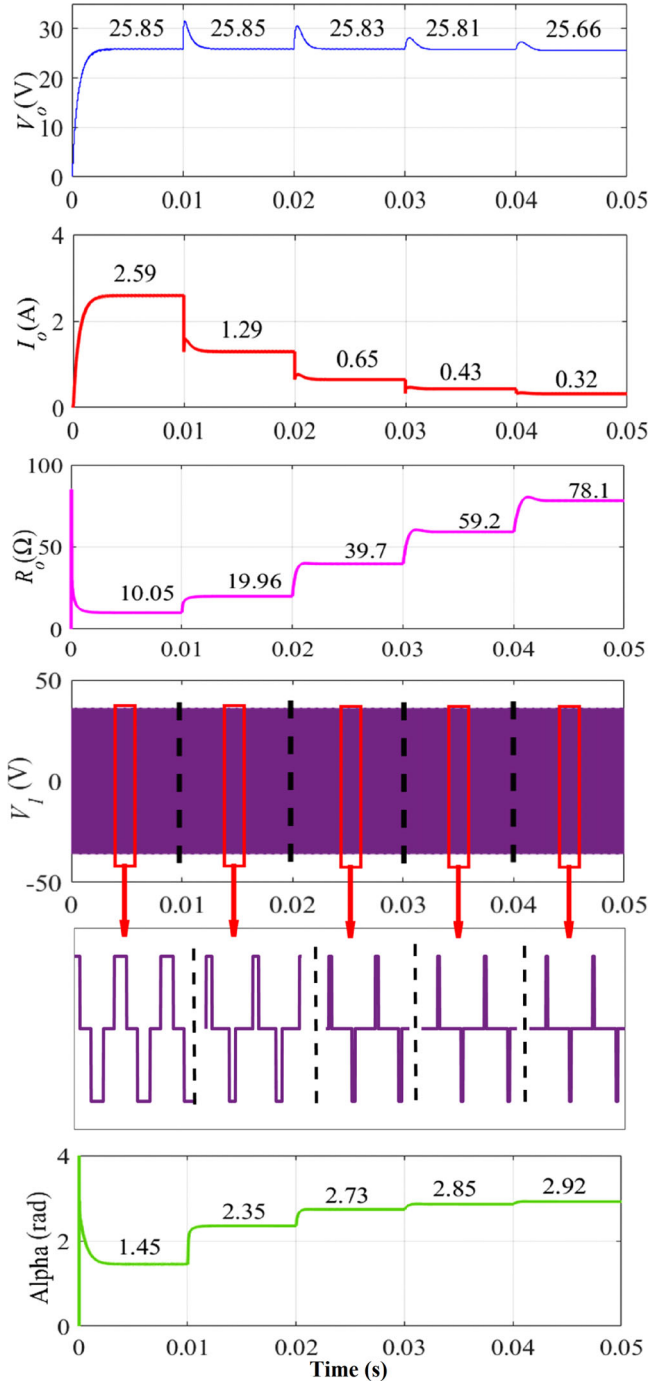


FIGURE 12 Simulation results of the closed-loop MPC scheme in the CV mode

control signal, and weight factors respectively. In this controller, to avoid the low-speed dynamic response of the systems, no restrictions are imposed ($\alpha(k) = 0$). Here the prediction horizon is limited to one-step ($N_p = 1$) in order to reduce the computational burden. This control horizon is suitable for voltage and current tracking in power electronics systems [34]. The rest of the parameters are chosen as:

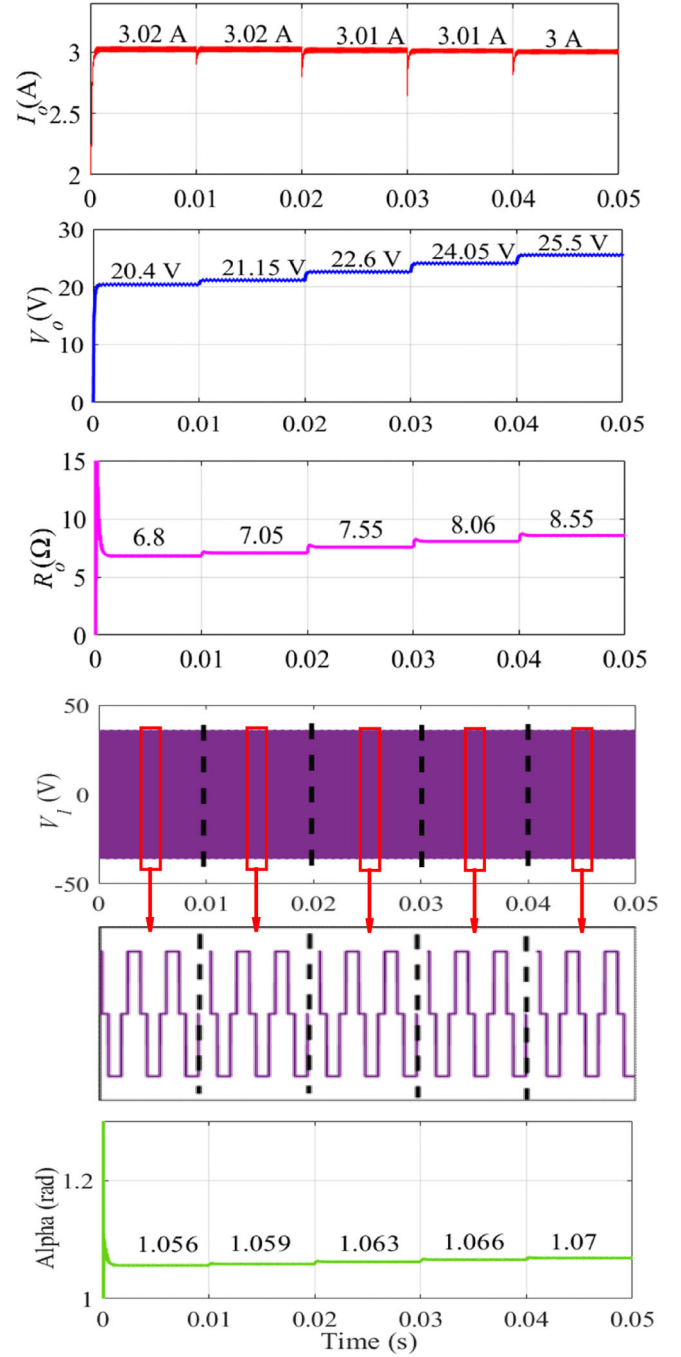


FIGURE 13 Simulation results of the closed-loop MPC scheme in the CC mode

$$N_1 = N_c = \lambda(k) = 1$$

$$\begin{aligned}
 J(N_1, N_p, N_c) &= \sum_{k=1}^1 [y(n+k) - w(n+k)]^2 \\
 &= [y(n+1) - w(n+1)]^2. \quad (19)
 \end{aligned}$$

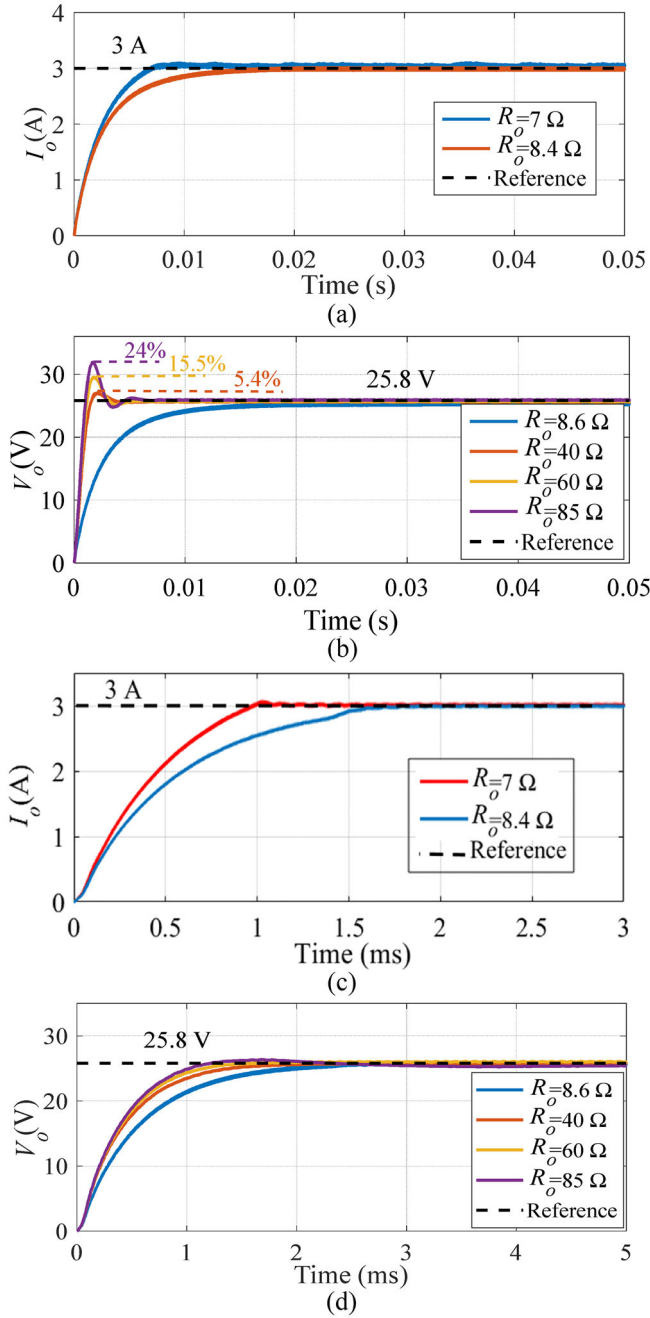


FIGURE 14 Simulation results of the start-up transient response in the CC/CV mode for (a) the CC mode with PI controller (b) the CV mode with PI controller (c) the CC mode with MPC scheme (d) the CV mode with MPC scheme

The J is a cost function that must be minimized. Minimizing the cost function implies:

$$\frac{\partial J(N_1, Np, Nc)}{\partial w} = 0.$$

$$y(n+1) = w(n+1). \quad (20)$$

$$\frac{\partial^2 J(Np, Nc)}{\partial w^2} = 2 > 0 \text{ minimum}$$

Because the second derivative of the cost function J is positive, it has the minimum value. By placing Equation (15) in Equations (16) and (17) and arranging it according to Equation (20), V_o and I_o are then calculated by:

$$I_o(n+1) = \frac{8\omega M * V_{dc} \cos\left(\frac{\delta(n+1)}{2}\right)}{\pi^2 \left(R_1 + \frac{\omega^2 M^2}{R_2 + \frac{8}{\pi^2} R_o(n)} \right) \sqrt{\left(\frac{\omega^2 L_2 C_2 - 1}{\omega C_2} \right)^2 + \left(R_2 + \frac{8}{\pi^2} R_o(n) \right)^2}}. \quad (21)$$

$$V_o(n+1) = \frac{8R_o(n) \omega M * V_{dc} \cos\left(\frac{\delta(n+1)}{2}\right)}{\pi^2 \left(R_1 + \frac{\omega^2 M^2}{R_2 + \frac{8}{\pi^2} R_o(n)} \right) \sqrt{\left(\frac{\omega^2 L_2 C_2 - 1}{\omega C_2} \right)^2 + \left(R_2 + \frac{8}{\pi^2} R_o(n) \right)^2}}. \quad (22)$$

To obtain the optimal delta to control the WPT system in CC and CV mode, Equations (21) and (22) are arranged in terms of delta as:

$$\delta_{I_o}(n+1) = 2\cos^{-1} \left[\frac{V_o(n+1) \pi^2 \left(R_1 + \frac{\omega^2 M^2}{R_2 + \frac{8}{\pi^2} R_o(n)} \right) \sqrt{\left(\frac{\omega^2 L_2 C_2 - 1}{\omega C_2} \right)^2 + \left(R_2 + \frac{8}{\pi^2} R_o(n) \right)^2}}{8\omega M V_{dc}} \right] \quad (23)$$

$$\delta_{V_o}(n+1) = 2\cos^{-1} \left[\frac{I_o(n+1) \pi^2 \left(R_1 + \frac{\omega^2 M^2}{R_2 + \frac{8}{\pi^2} R_o(n)} \right) \sqrt{\left(\frac{\omega^2 L_2 C_2 - 1}{\omega C_2} \right)^2 + \left(R_2 + \frac{8}{\pi^2} R_o(n) \right)^2}}{8R_o(n) \omega M V_{dc}} \right] \quad (24)$$

4.2 | Algorithm description

As shown in Figure 10, the active power P_1 and the $I_{1,rms}$ are calculated by the measured voltage and current through the primary side sensors. The P_1 and the $I_{1,rms}$ are placed in the Equation (14) to estimate the R_o . By estimating the R_o , the value of the I_o is calculated from Equation (16). If the output current exceeds the nominal value of the battery current $I_{o,n}$, the controller selects CC mode, otherwise the controller selects CV mode. In the CC and CV mode, the $\delta_{I_o}(n+1)$ and $\delta_{V_o}(n+1)$ are obtained through Equations (23) or (24), respectively.

The optimum δ is given to the block of the phase shift algorithm to be translated to the optimum duty cycle. Finally, the optimum duty cycle is given to the H-bridge inverter's switches. When the charging current I_o reaches below $0.1 I_{ref}$, it means

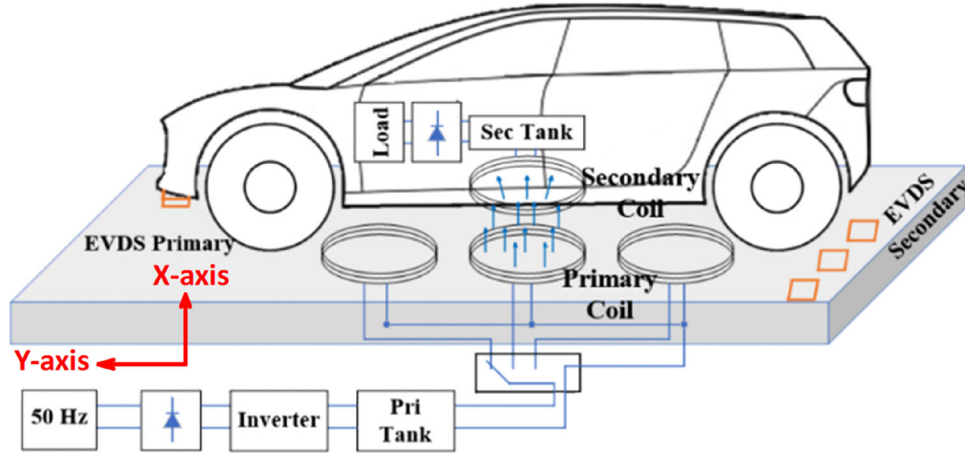


FIGURE 15 A WPT system and EVDS in DWC charging application

that the battery is fully charged and the charging process stops. For protection purposes, in the absence of the receiver pad, the circuit is switched off to prevent the current increase.

5 | SIMULATION RESULT AND DISCUSSION

5.1 | Primary-side MPC scheme

Table 1 shows the parameters of the WPT system in the CC/CV mode charge.

The output voltage and current in open-loop condition, with load variation from 6.75 to 85 Ω are shown in Figure 11. The V_o and I_o increase to 250 V and 3.5 A, respectively, which are much higher than the rated value of the battery and damage it.

5.2 | Verified the proposed controller with simulation results

The results of the simulation are shown in following figures which verify the suitable performance of the proposed MPC. Figure 12, shows the WPT system in the CV charging mode. According to Figure 12, by increasing the R_o from 10.05 to 78.1 Ω , the V_o approximately remains constant about 25.8 V. By the abovementioned variation in the R_o , the I_o decreases from 2.59 to 0.32 A. Figure 13 shows the output current in CC mode. It can be seen that by increasing the R_o from 6.8 to 8.55 Ω , the output current approximately remains constant about 3A. By the aforementioned change in the R_o , the output voltage increases from 20.4 to 25.5 V.

Figure 14 shows the start-up transient of voltage and current when the system works in CC/CV mode by the PI controller and the proposed MPC scheme. The percentage of overshoot and settling time for PI and MPC in $R_o = 7, 8.4, 8.6, 40, 60$ and 85 Ω are shown in Table 2. Based on Table 2 the proposed

controller for all the loads was significantly faster and smoother than PI controller.

The li-ion battery is highly sensitive to overvoltage [10], so the WPT system must reach the steady state response without overshoot. On the other hand, in the dynamic charging method, due to instantaneous changes in parameters such as load and mutual inductance, the WPT system must be able to respond appropriately and quickly to the presence and position of the EV (Turn on the system and compensate M changing). As a result, it is essential for the WPT system to have a smooth and fast response.

By increasing or decreasing the response speed of the PI controller by changing controller parameters (K_p, K_i), the system leaves the optimal state and the system experiences overshoot or slow response. In the studied system, the load and mutual inductance are variable, while the PI controller has constant coefficients (K_p, K_i) and cannot provide a desirable response for complete range of load and mutual inductance variation. So the system responses with PI controller will not be optimal for different loads and mutual inductance. According to Figure 14c,d, the MPC scheme has much lower overshoot and faster dynamic response in comparison to PI controller. In fact, the ability to generate and apply the optimal control signal (for complete load and mutual inductance variation) to the WPT system, MPC gives better results comparing to PI [26].

5.3 | Misalignment compensation

There are two types of misalignments between transmitter and receiver coils in a WPT system: One along the X -axis and the other along the Y -axis. The DD coils mutual inductance variation due to misalignments along the Y -axis is small and nearly negligible (Figure 6) [1]. Therefore, it is enough to turn on the WPT system when the car reaches the desired range in terms of mutual inductance ($M = M_{\text{nominal}}$). But the mutual inductance changes along the X -axis is considerable. Consequently, if not compensated, the charging process will run into problem. In

this regard, the EV detection system (EVDS) is used to detect the presence of a vehicle as well as the amount of misalignment in the X -axis direction. Schematic of an EVDS is shown in Figure 15, which shows three secondary windings and a primary winding. The primary EVDS winding is mounted beneath the vehicle and the secondary EVDS windings are mounted along the road, in front of the primary winding of the WPT system. In fact, the EV position along the X -axis is detected by the EVDS. Then, the output signal of the sensor will be applied to the control algorithm. Thus, the mutual inductance in the algorithm is corrected. In terms of alignment and misalignment in the X -axis direction, the mutual inductance is $M = M_{\text{nominal}}$ and $M < M_{\text{nominal}}$, respectively.

In order to evaluate the capability of the proposed control strategy to track the mutual inductance changes, system performance at CC and CV modes ($R_o = 8$ and 30Ω) before and after X -axis misalignment are simulated. System dynamic performance simulation is carried out and compared for proposed MPC and PI controller. Simulation results are shown in Figure 16.

As shown in the Figure 16, by changing the mutual inductance from the nominal value of $15.36 \mu\text{H}$ to the value of $12 \mu\text{H}$, the value of I_o remains constant at the nominal value of 3A after passing the instantaneous changes of 0.5 ms. In addition, changes in mutual inductance from 11 to $16 \mu\text{H}$ have been performed. By changing the mutual inductance, the value of V_o remains constant at the nominal value of 25.8 V after passing a transient response lasting 1 ms. It can be seen in transient state that due to the inductance changes, MPC scheme is 15 to 76 times faster than PI controller while its over-and undershoot are lower.

6 | EXPERIMENTAL RESULTS

6.1 | The WPT system experimental setup

As shown in the Figure 17, a 90 W prototype WPT system has been implemented just to verify the simulation results of the proposed MPC scheme with the parameters of Table 1. The MPC scheme is implemented using the DSP, TMS320F28335 chip. In the H-bridge inverter and rectifier, MOSFETs (Infineon IRFP15N60L) and ultra-fast diode (Fairchild FFA60UP30DN) are used, respectively. A Hall effect LEM (LA 55-P) current sensor and a MINMAX (MAU202) voltage sensor were used to measure current and voltage, respectively. The magnetic part of the WPT system consists of two DD transmitters and receiver pads. Each DD pad consists of two D-shape spiral sub-coils. To reduce the high-frequency skin and proximity effect losses, it is wound using litz wire (400×0.1 mm). Dimensions of the transmitter and receiver pads are identical, 400×400 mm². Each of the transmitter and receiver pads consist of two sub-coils that have $N_{sc1} = 11$, $N_{sc2} = 11$, $N_{sc3} = 6$, and $N_{sc3} = 6$ turns, respectively. To guide the magnetic flux, each DD pad has ten ferrite cores with dimensions of $120 \times 10 \times 8$ mm³. The load consists of two 54Ω series variable potentiometers.

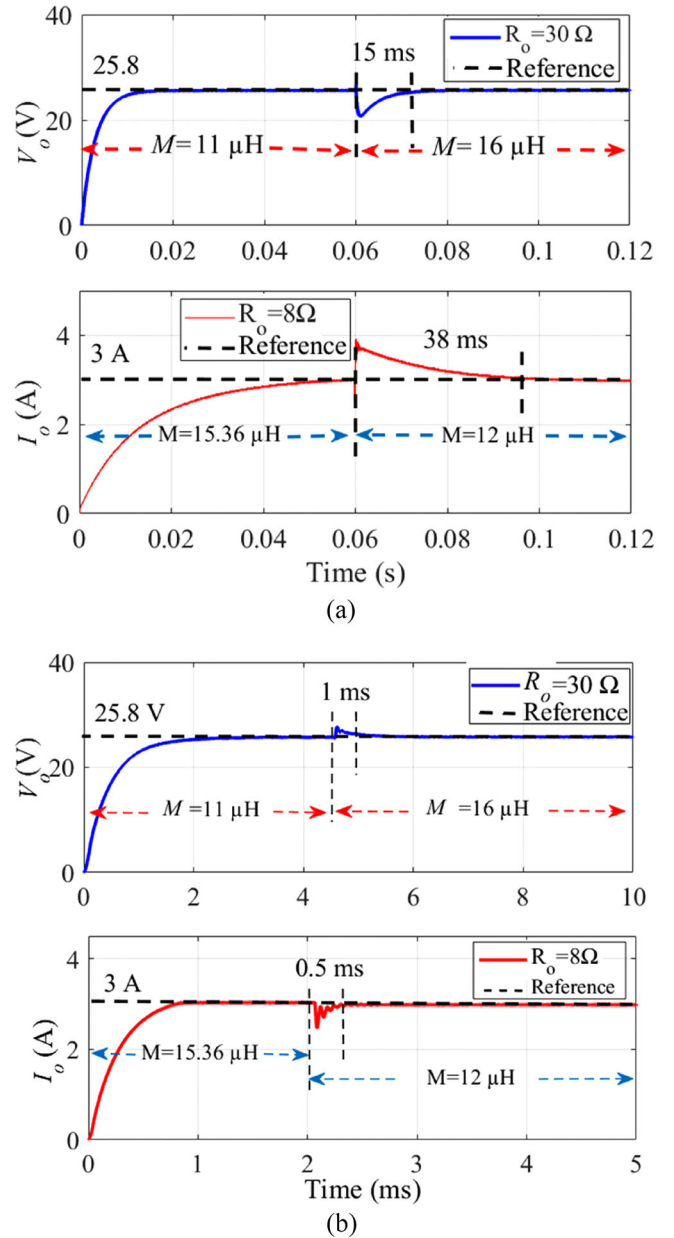


FIGURE 16 The effect of M changes on I_o and V_o (a) PI controller (b) MPC scheme



FIGURE 17 Photo of the WPT system experimental setup

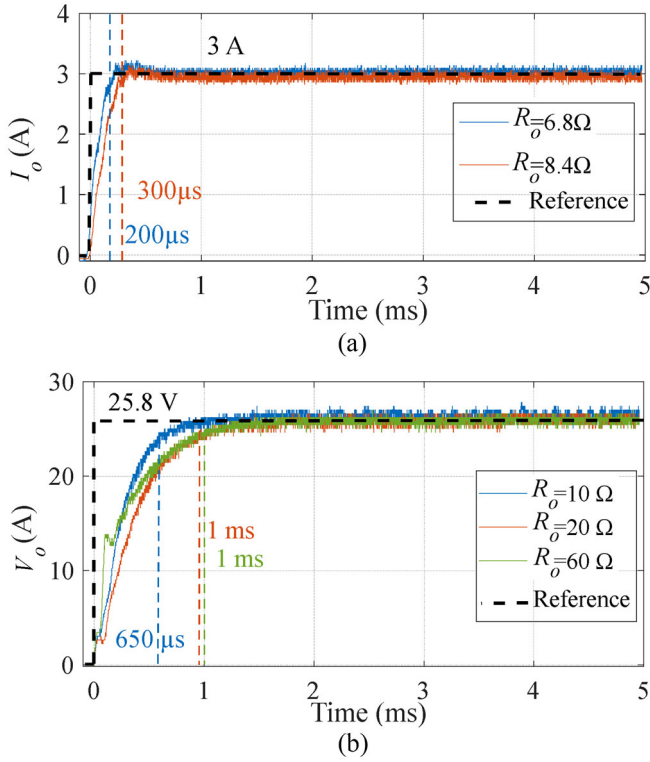


FIGURE 18 Experimental results of the start-up transient response (a) I_o in CC mode (b) V_o in CV mode

6.2 | Transient start-up dynamic

Figure 18a,b shows the transient response of the experimental testbed for different loads ($R_o = 6.8, 8.4, 10, 20, 60 \Omega$) in CC and CV charge modes. From Figure 18a, it can be seen that the settling time for the I_o in CC mode is less than $300 \mu\text{s}$ (Figure 18a) and the settling time for the V_o in CV mode is less than 1 ms (Figure 18b).

As shown in Figure 19, by changing the R_o from 44.1 to 22.5Ω , the V_o value with an error of less than 0.5% remains constant with respect to the reference value in CV mode. It can be seen that by changing the output resistance from 44.1 to 22.5 and 44.1Ω , the transient response time of the V_o is lower than 0.6 ms. Also, as shown in Figure 19 the transient response time periods of the I_o for the abovementioned load changes are 0.6 ms and $5 \mu\text{s}$.

7 | CONCLUSION

This paper proposed a primary-side MPC scheme that executes the CC/CV protocol with a fast and smooth dynamic transient response compared to the conventional PI controller for the WPT system. The proposed controller settling times are 2.62 to 15.2 times (depending on battery SOC) faster than the PI controller. By changing the load resistance from 44.1 to 22.5 and 44.1Ω , the output voltage and current adjustment time is lower than 0.6 ms. In DWC application the EV frequently (with a fast

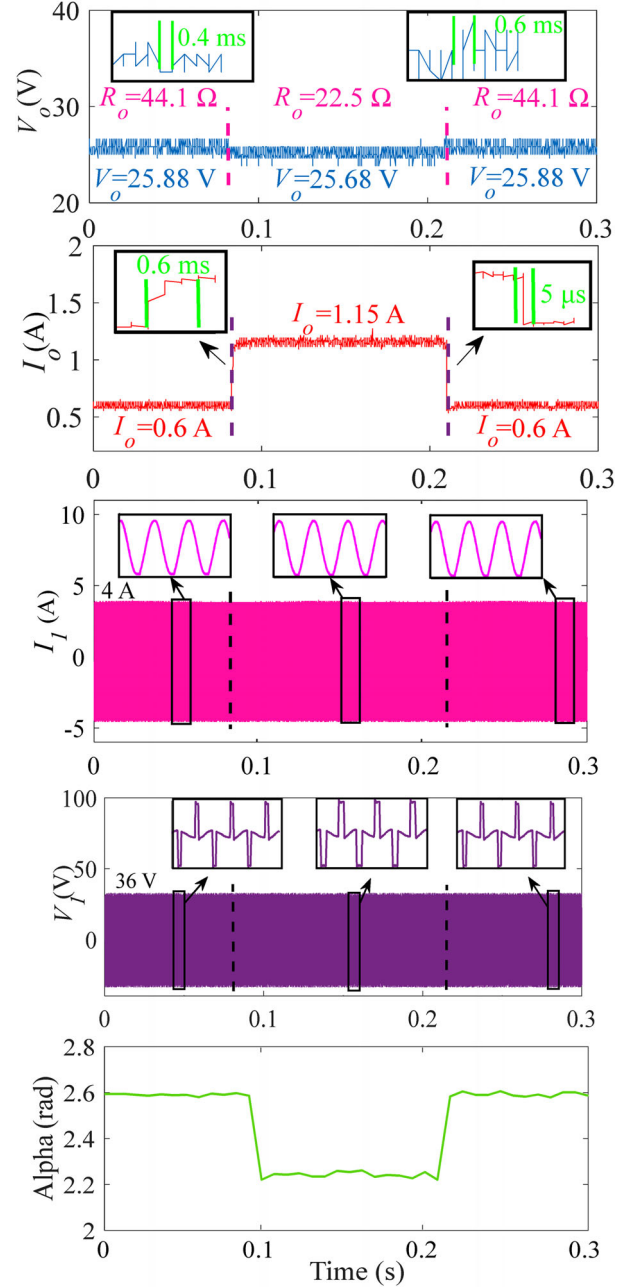


FIGURE 19 Experimental results of the transient load changing in CV mode

speed) passes the WPT transmitter pads. As a result, fast turn on/off of the WPT system both increase the transmitted power to the EV and the efficiency of the transmitter section of the WPT system. Since the battery of the EV is Li-ion, 24% voltage overshoot in the PI controller responses could damage the battery, while the maximum overshoot in the responses of the proposed controller is 2.3%. To eliminate the communication link, the output load is estimated, therefore system stability and simplicity are guaranteed. The efficiency of the implemented system is 76.5%. The proposed controller is simple, based on the optimal control law and it doesn't need any gain tuning that makes it a potential candidate for DWC of EVs.

CONFLICT OF INTEREST

There is no Conflict of Interest statement.

ORCID

Seyed Ehsan Abdollahi  <https://orcid.org/0000-0003-2277-1060>

REFERENCES

- Li, S., Mi, C.C.: Wireless power transfer for electric vehicle applications. *IEEE J. Emerg. Sel. Top. Power Electron.* 3(1), 4–17 (2014)
- Li, P., Bashirullah, R.: A wireless power interface for rechargeable battery operated medical implants. *IEEE Trans. Circuits Syst. II Express Briefs* 54(10), 912–916 (2007)
- Waters, B.H., Sample, A.P., Bonde, P., Smith, J.R.: Powering a ventricular assist device (VAD) with the free-range resonant electrical energy delivery (FREE-D) system. *Proc. IEEE* 100(1), 138–149 (2011)
- Hoang, H., Lee, S., Kim, Y., Choi, Y., Bien, F.: An adaptive technique to improve wireless power transfer for consumer electronics. *2012 IEEE Int. Conf. Consum. Electron. (ICCE)* 58(2), 327–332 (2012)
- Kuo, R.-C., Riehl, P., Satyamoorthy, A., Plumb, W., Tustin, P., Lin, J.: A 3D resonant wireless charger for a wearable device and a mobile phone. In: *2015 IEEE Wireless Power Transfer Conference (WPTC)*, Boulder, Colorado, pp. 1–3 (2015)
- Deyle, T., Reynolds, M.: Surface based wireless power transmission and bidirectional communication for autonomous robot swarms. In: *2008 IEEE International Conference on Robotics and Automation*, Pasadena, California, pp. 1036–1041 (2008)
- Scheible, G., Schutz, J., Apneseth, C.: Novel wireless power supply system for wireless communication devices in industrial automation systems. In: *IEEE 2002 28th Annual Conference of the Industrial Electronics Society. IECON 02*, vol. 2, Seville, Spain, pp. 1358–1363 (2002)
- Ramezani, A., Farhangi, S., Iman-Eini, H., Farhangi, B., Rahimi, R., Moradi, G.R.: Optimized LCC-series compensated resonant network for stationary wireless EV chargers. *IEEE Trans. Ind. Electron.* 66(4), 2756–2765 (2018)
- Fujita, T., Yasuda, T., Akagi, H.: A dynamic wireless power transfer system applicable to a stationary system. *IEEE Trans. Ind. Appl.* 53(4), 3748–3757 (2017)
- Choi, S.S., Lim, H.S.: Factors that affect cycle-life and possible degradation mechanisms of a Li-ion cell based on LiCoO₂. *J. Power Sources* 111(1), 130–136 (2002)
- Song, K., Li, Z., Jiang, J., Zhu, C.: Constant current/voltage charging operation for series-series and series-parallel compensated wireless power transfer systems employing primary-side controller. *IEEE Trans. Power Electron.* 33(9), 8065–8080 (2017)
- Gati, E., Kampitsis, G., Manias, S.: Variable frequency controller for inductive power transfer in dynamic conditions. *IEEE Trans. Power Electron.* 32(2), 1684–1696 (2016)
- Tran, D.H., Choi, W.: Design of a high-efficiency wireless power transfer system with intermediate coils for the on-board chargers of electric vehicles. *IEEE Trans. Power Electron.* 33(1), 175–187 (2017)
- Qu, X., Han, H., Wong, S.-C., Chi, K.T., Chen, W.: Hybrid IPT topologies with constant current or constant voltage output for battery charging applications. *IEEE Trans. Power Electron.* 30(11), 6329–6337 (2015)
- Mai, R., Chen, Y., Li, Y., Zhang, Y., Cao, G., He, Z.: Inductive power transfer for massive electric bicycles charging based on hybrid topology switching with a single inverter. *IEEE Trans. Power Electron.* 32(8), 5897–5906 (2017)
- Li, Z., Wei, G., Dong, S., Song, K., Zhu, C.: Constant current/voltage charging for the inductor-capacitor-inductor-series compensated wireless power transfer systems using primary-side electrical information. *IET Power Electron.* 11(14), 2302–2310 (2018)
- Tavakoli, R., Pantic, Z.: Analysis, design, and demonstration of a 25-kW dynamic wireless charging system for roadway electric vehicles. *IEEE J. Emerg. Sel. Top. Power Electron.* 6(3), 1378–1393 (2017)
- Yang, Y., Zhong, W., Kiratipongvoot, S., Tan, S.-C., Hui, S.Y.R.: Dynamic improvement of series-series compensated wireless power transfer systems using discrete sliding mode control. *IEEE Trans. Power Electron.* 33(7), 6351–6360 (2017)
- Hu, X., Wang, Y., Jiang, Y., Lei, W., Dong, X.: Maximum efficiency tracking for dynamic wireless power transfer system using LCC compensation topology. In: *2018 IEEE Energy Conversion Congress and Exposition (ECCE)*, Portland, Oregon, pp. 1992–1996 (2018)
- Song, K., Li, Z., Jiang, J., Zhu, C.: Constant current/voltage charging operation for series-series and series-parallel compensated wireless power transfer systems employing primary-side controller. *IEEE Trans. Power Electron.* 33(9), 8065–8080 (2017)
- Shi, W., Deng, J., Wang, Z., Cheng, X.: The start-up dynamic analysis and one cycle control-PID control combined strategy for primary-side controlled wireless power transfer system. *IEEE Access* 6, 14439–14450 (2018)
- Jiang, J., Song, K., Li, Z., Zhu, C., Zhang, Q.: System modeling and switching control strategy of wireless power transfer system. *IEEE J. Emerg. Sel. Top. Power Electron.* 6(3), 1295–1305 (2018)
- Gheisarnejad, M., Farsizadeh, H., Tavana, M.-R., Khooban, M.H.: A novel deep learning controller for DC/DC buck-boost converters in wireless power transfer feeding CPLs. *IEEE Trans. Ind. Electron.* 68, 6379–6384 (2020)
- Rodriguez, J., et al.: State of the art of finite control set model predictive control in power electronics. *IEEE Trans. Ind. Inf.* 9(2), 1003–1016 (2012)
- Mohamed, A.A., Mohammed, O.: Bilayer predictive power flow controller for bidirectional operation of wirelessly connected electric vehicles. *IEEE Trans. Ind. Appl.* 55(4), 4258–4267 (2019)
- Liu, S., et al.: Dynamic improvement of inductive power transfer systems with maximum energy efficiency tracking using model predictive control: Analysis and experimental verification. *IEEE Trans. Power Electron.* 35(12), 12752–12764 (2020)
- Qi, C., Lang, Z., Su, L., Chen, X., Miao, H.: Model predictive control for a bidirectional wireless power transfer system with maximum efficiency point tracking. In: *2019 IEEE International Symposium on Predictive Control of Electrical Drives and Power Electronics (PRECEDE)*, Quanzhou, China, pp. 1–5 (2019)
- Patil, D., McDonough, M.K., Miller, J.M., Fahimi, B., Balsara, P.T.: Wireless power transfer for vehicular applications: Overview and challenges. *IEEE Trans. Transp. Electrification* 4(1), 3–37 (2017)
- Schneider, J.J.S.I.J.T.: Wireless power transfer for light-duty plug-in/electric vehicles and alignment methodology. (2016)
- Hayt, W.H. Jr., Kemmerly, J.E., Durbin, S.M.: *Engineering Circuit Analysis*, 8th ed., McGraw-Hill Higher Education, New York (2006)
- Chapman, S.J.: *Electric Machinery Fundamentals*, 5th ed., McGraw-Hill, inc, New York (2012)
- Li, S., Mi, C.C.: Wireless power transfer for electric vehicle applications. *IEEE J. Emerg. Sel. Top. Power Electron.* 3(1), 4–17 (2014)
- Vazquez, S., Rodriguez, J., Rivera, M., Franquelo, L.G., Norambuena, M.: Model predictive control for power converters and drives: Advances and trends. *IEEE Trans. Ind. Electron.* 64(2), 935–947 (2016)
- Garayalde, E., Aizpuru, I., Iraola, U., Sanz, I., Bernal, C., Oyarbide, E.: Finite control set MPC vs continuous control set MPC performance comparison for synchronous buck converter control in energy storage application. In: *2019 International Conference on Clean Electrical Power (ICCEP)*, Otranto, Italy, pp. 490–495 (2019)

How to cite this article: Alkasir, A., Abdollahi, S. E., Abdollahi, S. R., Wheeler, P.: Enhancement of dynamic wireless power transfer system by model predictive control. *IET Power Electron.* 1–13 (2021) <https://doi.org/10.1049/pel2.12213>.